

Polarized synchrotron data and the structure of the Galactic magnetic field

C. T. Becker and M. Kachelrieß
Institutt for fysikk, NTNU, Trondheim, Norway
(Dated: August 3, 2024)

The polarized synchrotron data of the northern C-BASS survey show a surprisingly low linear polarization fraction, $\langle \Pi \rangle \simeq 3\%$, while the magnetic field polarization features coherent structures over rather large angular scales. The low polarization degree points to a strong dominance of the turbulent magnetic field—in agreement with the observation that the total synchrotron intensity is much larger than expected from the regular component in current models for the Galactic magnetic field (GMF). In contrast, studies of cosmic ray propagation employing these GMF models suggest that cosmic rays propagate anisotropically, what in turn requires weak turbulent fields. As a solution to this contradicting requirements, we suggest that the GMF consists of three components with different levels of turbulence: a disk dominated by the turbulent field, a halo dominated by the regular field, plus an extended turbulent halo field.

I. INTRODUCTION

Galaxies are permeated by magnetic fields with strengths of the order of μG . These magnetic fields have not only a major impact on the evolution of galaxies but are also responsible for the deflection and the confinement of cosmic rays (CR) [1, 2]. In turn, the synchrotron emission of CR electrons is a key signature both of CRs themselves and of magnetic fields. In general, magnetic fields can be split into a regular, average component \mathbf{B} and a chaotic, turbulent component \mathbf{b} with $\langle \mathbf{b} \rangle = 0$. While the average $\langle \cdot \rangle$ is formally an ensemble average, observationally it has to be replaced by an average over, e.g., different regions which are statistically independent and subject to similar physical conditions.

Faraday Rotation Measures (RMs) of Galactic and extragalactic polarized radio sources provide important information on the Galactic magnetic field (GMF). They are proportional to the line-of-sight integral of the product of the thermal electron density n_e of the interstellar medium and the magnetic field parallel to the line-of-sight, $\text{RM} \propto \int_0^L n_e(s) [B_{\parallel}(s) + b_{\parallel}(s)] ds$, where L is the distance to the source. Another important source of information on the GMF is the synchrotron radiation emitted by relativistic CR electrons. Sky maps of the Stokes parameters Q and U of the polarized synchrotron emission from the Galaxy were extracted from the data of the WMAP and Planck satellites. These parameters encode the orientation of the transverse component of the magnetic field. The strength of the polarized emission, $P = \sqrt{Q^2 + U^2}$ is again given by a line-of-sight integral, approximately given by $P \propto \int_0^L n_{\text{cr,e}}(s) [B_{\perp}^2(s) + b_{\perp}^2(s)] ds$, where $n_{\text{cr,e}}$ denotes the density of cosmic-ray electrons. The total intensity, I , follows from a similar relation.

Thus, RM and radio sky maps provide complementary data on B_{\parallel} and B_{\perp} and, having enough tracers along the line-of-sight, one may attempt to reconstruct the three-dimensional structure of the GMF. Assuming, as it is often done, that the contribution of the turbulent field \mathbf{b} cancels completely in the RM and the polarized intensity P allows one to disentangle also the regular and turbulent

components of the field. However, the morphology of current models of the GMF like those of Refs. [3–7] differ substantially, although they reproduce the Faraday RM data and synchrotron emission maps to which they were fitted. This implies in particular that it is at present not possible to derive a unique best-fit model for the GMF. In order to illustrate at least partially the currently allowed parameter space of these models, the authors of Ref. [6] presented therefore recently not a single but a suite of eight GMF models.

Another sign for the inconsistency of current GMF models is that fits to either RMs or synchrotron data yield conflicting results: The overall magnetic field strengths derived from RMs are a factor few smaller than from synchrotron emission. Explanations for this discrepancy include the existence of anisotropic random fields contributing to P but not to RM, or an anti-correlation of n_e and B leading to an underestimation of B from RMs [8]. An additional source of uncertainties in the GMF models are deficiencies in the models for the three-dimensional densities of thermal and CR electrons. In particular, the latter are not modeled self-consistently together with the GMF but are derived using an independent and over-simplified diffusion frame-work.

In this work, we do not aim to improve relative to existing GMF models. Instead, we show how three seemingly contradicting observations—the recent polarization data from the C-Band All-Sky Survey (C-BASS) [9, 10], constraints from CR escape [11–13], and the slow diffusion found close to some TeV pulsar-wind nebula (PWN) like Geminga [14]—can be explained and matched to different elements of a schematic GMF model. After reviewing these observations, we present our schematic model and derive the expected polarization degree towards the Galactic north pole and the latitude profile of the synchrotron intensity. We obtain an acceptable agreement with the data for a model consisting of three components with different levels of turbulence: a disk dominated by a turbulent field with small coherence length, a halo dominated by the regular field, plus an extended turbulent halo field.

II. C-BASS POLARIZATION DATA

The C-BASS collaboration aims to obtain an all-sky map of the Galactic synchrotron emission at 5 GHz in both total intensity and polarization. Preliminary results of the northern C-BASS instrument were presented in Refs. [9, 10]. The minimal distortions caused by Faraday rotation at this frequency and the higher signal-to-noise ratio compared to the WMAP and Planck surveys made for the first time an accurate separation of the synchrotron from other emission processes possible. In the northern high latitudes, $b > 30^\circ$, and excluding Loop I and III, an average linear polarization degree of $\langle \Pi \rangle \equiv \langle P/I \rangle \simeq 3.3\%$ was reported, with only few pixels exceeding 10%. This low values should be contrasted with the expectation of $\Pi = (1+p)/(7/3+p) = 75\%$ for a regular, uniform magnetic field and a power-law energy distribution $dN/dE \propto E^{-p}$ of CR electron energies with $p = 3$.

In addition, results for the two-point angular correlation function $D(\vartheta) = \langle \chi(\mathbf{n}) - \chi(\mathbf{n}') \rangle$ of the relative orientation χ of the local polarization basis were presented in Refs. [9, 10]. The shape of the two-point correlation function $D(\vartheta)$, where ϑ is the angle between the unit vectors \mathbf{n} and \mathbf{n}' , indicates that the typical angular size of field structures is around $\vartheta_0 \simeq 15^\circ$. Using a simple cell model for a purely turbulent field, where one identifies the cell size L with the coherence length L_c of the turbulent field, one expects $\sin(\vartheta_0/2) \simeq 1/N$ for a line-of-sight with length NL . Assuming then a random walk for the orientation χ , the scale $\vartheta_0 \simeq 15^\circ$ implying $\mathcal{O}(N) \sim 10$ cells leads to $\Pi \simeq 0.75/\sqrt{10} \simeq 24\%$ [9]. Thus there is a contradiction between the observed coherence of the magnetic field polarization over rather large angular scales and the low polarization degree in the C-BASS data. Adding a regular field would strengthen the discrepancy.

We can quantify this disagreement calculating the linear polarization degree for the suite of GMF models recently presented in Ref. [6], adding a turbulent random field normalized by $b(\mathbf{x}) = \eta B(\mathbf{x})$. We choose the coherence length as $L_c = 20$ pc and $p = 2.8$ as slope of the electron energy distribution. In Table I, we report the expectation value of $\langle \Pi \rangle$ towards the Galactic north pole. We see that the variation in $\langle \Pi \rangle$ between different models for the regular field is very small. Increasing η , the average polarization degree decreases until it flattens out at $\langle \Pi \rangle \simeq 0.12$ for $\eta \gg 1$. Even lower polarization levels would require smaller values of the coherence length. Thus the measured polarization degree requires a strong dominance of the turbulent field and small coherence lengths, in contradiction to the large angular size of the observed polarization features.

| η | base | neCL | expX | spur | cre10 | synCG | twistX | nebCor |
|--------|------|------|------|------|-------|-------|--------|--------|
| 1 | 0.36 | 0.37 | 0.36 | 0.39 | 0.33 | 0.39 | 0.36 | 0.35 |
| 1.5 | 0.22 | 0.23 | 0.22 | 0.24 | 0.2 | 0.24 | 0.22 | 0.21 |
| 10 | 0.12 | 0.12 | 0.12 | 0.12 | 0.12 | 0.12 | 0.12 | 0.12 |

TABLE I: The average linear polarization degree $\langle \Pi \rangle$ for the eight GMF models from Ref. [6] plus a turbulent field with strength $b = \eta B$.

III. COSMIC RAY ESCAPE

A. Isotropic diffusion

The large majority of studies on CR propagation in the Milky Way employs a phenomenological approach, using an isotropic diffusion coefficient $D(\mathcal{R})$ uniform in a cylinder enclosing the Galactic disk. Its dependence on rigidity $\mathcal{R} = cp/(ZeB)$ is typically parameterised by a (broken) power law, $D(\mathcal{R}) = D_0(\mathcal{R}/\mathcal{R}_0)^{-\delta}$. Then the parameters D_0 and δ are determined from fits to secondary-to-primary ratios as, e.g., boron-to-carbon and the abundance of radioactive secondaries as $^{10}\text{Be}/^9\text{Be}$. Typical values found from a combined fit to many observables using GALPROP [15, 16] are in the range $(5 - 8) \times 10^{28} \text{cm}^2/\text{s}$ at the reference rigidity $\mathcal{R}_0 = 4$ GV with the high-energy slope $\delta = 0.34 - 0.36$. Note that this slope is very close to the expectation $\delta = 1/3$ for a Kolmogorov power spectrum of the turbulent magnetic field. Similar values for D_0 and δ are found using other CR diffusion codes like, e.g., DRAGON [17, 18].

In the picture of an uniform diffusion coefficient, one can model the propagation of CRs as a random walk with an energy dependent effective step size L_0 . For a pure isotropic random field, one expects as functional dependence of the diffusion coefficient

$$D_{\text{iso}} = \frac{cL_0}{3} [(R_L/L_0)^{2-\gamma} + (R_L/L_0)^2], \quad (1)$$

where $R_L = \mathcal{R}/B = cp/(ZeB)$ is the Larmor radius of the CR and the condition $R_L(E_{\text{tr}}) = L_0$ determines the transition from small-angle scattering with $D(E) \propto E^2$ to large-angle scattering with $D(E) \propto E^{2-\gamma}$ and $\gamma = 5/3$ for a Kolmogorov power spectrum.

The numerical value of L_0 should scale with the correlation length as $L_0 \propto L_c$, but the proportionality factor has to be determined numerically. In Refs. [13, 19], it was found that $L_0 \simeq L_c/(2\pi)$ provides a good fit to their numerical results for isotropic Kolmogorov turbulence. For values of the field strength and correlation length expected for the GMF, the predicted diffusion coefficient from Eq. (1) is a factor of order 100 smaller than those extracted using, e.g., Galprop [15, 16] or DRAGON [17, 18]. A similar discrepancy was found earlier performing analytical estimates, but was considered to be within the error range expected for the approximations made [20].

However, a factor 100 difference in the diffusion coefficient leads to dramatic consequences for the GMF pa-

parameters: The weak field dependence of $D(E) \propto B^{-1/3}$ requires a reduction of B by a factor $1/100^3 = 10^{-6}$ for Kolmogorov turbulence keeping L_c constant. Keeping instead $B \sim \text{few} \times \mu\text{G}$, the correlation length should be comparable to the size of the Galactic halo. Therefore, it was concluded in Ref. [13] that CR escape is inconsistent with isotropic diffusion. This implies in turn that the regular field should dominate in the regions relevant for the CR escape from the Galactic disk.

B. Anisotropic propagation in GMF models

For a given GMF model, the propagation of CRs in the Milky Way can be studied also directly integrating the Lorentz equation. Calculating then observables like the grammage crossed by CRs or their escape time allows one to cross-check the viability of this GMF model. Since this approach is at low energies computationally expensive, it has been restricted to either relatively high energies [21] or young sources [22]. In Refs. [11, 12], the trajectory approach was applied for the first time to calculate the diffuse flux of CR primaries below the knee, using as lowest rigidity $\mathcal{R} = 10^{14}$ V. The authors calculated the grammage X crossed by CRs before escape in the Pshirkov et al. [3] and Jansson-Farrar (JF) models [4, 23] for the regular GMF together with a turbulent component with a Kolmogorov power-spectrum. They confirmed at the lowest rigidities the dependence $X \propto \mathcal{R}^{-1/3}$ expected in the large-angle scattering regime for Kolmogorov turbulence. This allowed them to connect their results to the observations at lower energies, especially to those from the AMS-02 collaborations [24]. In order to obtain agreement with these measurements, they had to reduce the strength of the turbulent field. As a result of this reduction, the low anisotropy level lead to strongly anisotropic propagation of CRs.

Anisotropic diffusion by itself, however, is not enough to facilitate the CR escape from the Galaxy: If the GMF model does not contain a poloidal component, only the CR transport along the plane towards either the Galactic bulge or its outer radial edge would be increased—what is too inefficient to reduce the grammage significantly [21]. This restriction is however not severe, since any realistic GMF model should contain a poloidal component, induced e.g. by Galactic winds and outflows. In the case of the JF model, its “X-field” leads to an additional tilt of the total magnetic field with respect to the Galactic plane.

We can estimate the level of anisotropy required to obtain consistency with the isotropic diffusion coefficient obtained fitting secondary ratios considering a simple toy model [13]. If the regular magnetic field in the halo has on average the tilt angle ϑ with the Galactic plane, the component of the diffusion tensor relevant for CR escape is given by

$$D_{zz} = D_{\perp} \cos(2\vartheta) + D_{\parallel} \sin(2\vartheta). \quad (2)$$

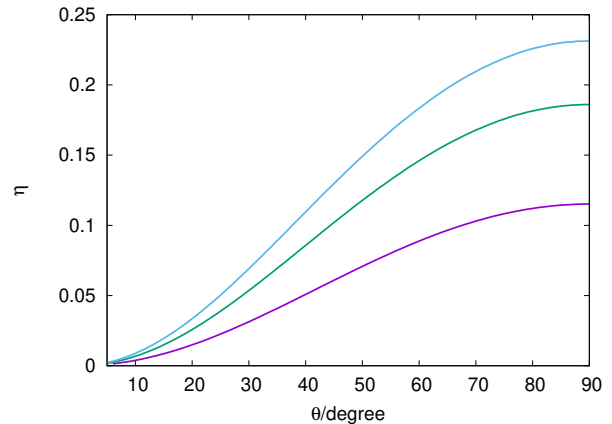


FIG. 1: The anisotropy level η as function of the tilt angle ϑ required for $D_{zz} = D_{\text{iso,obs}}$, for $\{L_{\text{max}}/\text{pc}, B/\mu\text{G}\}$ equal to $\{200, 3\}$ (top), $\{100, 3\}$ (middle) and $\{100, 4\}$ (down).

Requiring then $D_{zz} = D_{\text{iso}} = (5 - 8) \times 10^{28} \text{cm}^2/\text{s}$ as obtained with GALPROP [16] at $\mathcal{R}_0 = 4$ GV fixes η as function of the tilt angle ϑ . In Fig. 1, we show the resulting $\eta(\vartheta)$ relation for three different sets of values of the parameters L_{max} and B . Avoiding too small values of η clearly favors relatively large values of the coherence length. Still, the turbulence level η should be around or below 10% for a tilt angle $\vartheta \simeq 30^\circ$. Note that this level corresponds approximately to the one found propagating individual CRs in the JF model in Refs. [11, 12]. Moreover, the tilt of the total magnetic field with the Galactic plane induced by the X-field varies in the JF model between $\vartheta \simeq 10^\circ$ at Earth, increasing to $\vartheta \simeq 50^\circ$ further away from the Galactic plane. Thus an average tilt angle of $\vartheta \simeq 20^\circ - 30^\circ$ is a reasonable approximation to this model.

C. Isotropic diffusion close to PWNe

The diffusion coefficient deduced by the HAWC [14] collaboration for Geminga and PSR B0656+14 corresponds to $D = (2.1 \pm 0.6) \times 10^{26} \text{cm}^2/\text{s}$ at 10 GV, scaling to low energies using Kolmogorov turbulence. We can compare this value with the one predicted by the fitting formula (1) valid in the case of purely isotropic turbulence. Inserting numerical values appropriate for the HAWC measurement, it follows

$$D_{\text{iso}} \simeq 2 \times 10^{26} \frac{\text{cm}^2}{\text{s}} \left(\frac{\mathcal{R}}{10 \text{GV}} \right)^{1/3} \left(\frac{L_c}{2 \text{pc}} \right)^{2/3} \left(\frac{B}{4 \mu\text{G}} \right)^{-1/3}. \quad (3)$$

Thus the numerical value of the diffusion coefficient deduced from HAWC observations agrees with values expected from isotropic diffusion, for field strengths typical for the Galactic plane but relatively small coherence lengths.

This finding is in line with the results of Ref. [25].

These authors followed the trajectories of individual electrons in purely isotropic turbulence and compared the resulting gamma-ray emission to HAWC data, finding as best-fit value $b \simeq 3\mu\text{G}$ and small coherence lengths, $L_c \lesssim 5\text{pc}$. In principle, larger coherence lengths can be accommodated in Eq. (3) by increasing appropriately the field strength. However, as it was stressed first in Refs. [26, 27], CR propagation proceeds on scales smaller than $\text{few} \times L_c$ even in isotropic turbulence anisotropically, leading to a characteristic anisotropic source morphology. This argument was used in Ref. [25] to exclude larger coherence lengths.

Next we ask if one can avoid isotropic diffusion close to PWNe. Allowing for the presence of a regular magnetic field component close to PWNe leads to two consequences: On one hand, the perpendicular diffusion coefficient decreases, $D_\perp \leq D_{\text{iso}}$, opening in principle the possibility to reach the values indicated by Eq. (3). On the other hand, the parallel diffusion coefficient increases even faster, resulting in anisotropic diffusion and thus in general asymmetric source morphologies. Thus the problem of this scenario are again the resulting asymmetric source morphologies. Already for $\eta = 0.5$, the ratio $D_\parallel/D_\perp \simeq 100$ at 100 TeV [13] would imply a strongly anisotropic source morphology – with the source extension along the regular field direction much larger than deduced from HAWC observations. For a single source, such an asymmetry can be avoided if our line-of-sight to the source is by chance aligned with the regular magnetic field at the source. In the case of Geminga, one expects however a rather large angle between the line-of-sight and the regular magnetic field for any GMF model following mainly a spiral-like structure in the disk. Moreover, a search for asymmetries in the TeV halos around PWNe was conducted using Fermi-LAT data in Ref. [28]. No evidence for asymmetries was found. We thus conclude that observations favor isotropic diffusion of CRs close to PWNe, with values of the isotropic diffusion coefficient in line with expectation from simulations of test particle trajectories in such fields.

IV. STRUCTURE OF THE GALACTIC MAGNETIC FIELD

A. Three-component model

Let us now try to match the seemingly contradicting observations to different elements of a schematic GMF model. For this model, we suggest three main components, a disk, a halo and an extended halo which we will also call corona field:

- In order to ensure sufficient fast CR escape, we have to assume that the halo field is dominated by the regular field and that the sub-dominant turbulent component has a large coherence length L_c , such that $\sin(2\theta)D_\parallel \simeq D_0$ holds.

- In the disk, we assume that, at least locally, the magnetic field is dominated by the turbulent component and has a small L_c , such that $D \simeq D_{\text{iso}} \simeq D_0/100$ is valid. In this case, the number N of cells with coherence length L_c along a line-of-sight towards the Galactic North pole is $N = \mathcal{O}(10)$ in the disk and, thus, there will be only a partial cancellation of the contribution of the turbulent disk field to the polarization.

The dominance of the turbulent field could be either only a local anomaly, meaning that in the Local Bubble (and other super bubbles as well as close to some PWNe) diffusion is slow but otherwise not. Or, it could hold globally or at least in a large fraction of the disk. Since we test only line-of-sights starting at the Earth towards the Galactic North pole, we cannot distinguish between these two possibilities.

- Finally, we add an extended halo field: This field is also dominated by the turbulent component, but has a larger L_c , and may extend up to or beyond 200 kpc. This component will not contribute to the polarization, while adding emissivity to the total synchrotron intensity.

In the following, we will not attempt to construct a detailed GMF model consisting out of these three components. Instead, we will use these three components as a toy model to test if we can reproduce qualitatively the synchrotron and polarization data.

B. CR electron distribution

In addition to the magnetic field model, we require a model for the CR electron distribution $n_{\text{cr},e}(E, \mathbf{x})$. For the energy dependence and the normalization of the CR electron distribution in the Galactic disk, we use the local interstellar spectrum derived from the Voyager and AMS-02 data in Ref. [29]. In order to have simple formula for the synchrotron emissivity, we approximate the energy dependence by a power law, $dN/dE \sim E^{-p}$. Moreover, we assume factorization, $n_{\text{cr},e}(E, \mathbf{x}) = n(\mathbf{x})dN/dE$, and use an one-dimensional spatial picture. Thus we ignore a radial dependence of $n(\mathbf{x})$ and solve only for the z dependence. For an extended halo field with strength $B \simeq 0.5\mu\text{G}$, the characteristic electron energy to produce 5 GHz synchrotron radiation is $E_{\text{cr}} \simeq 12\text{GeV}$. At these energies, advection, energy losses due to synchrotron radiation and inverse Compton scattering, and energy gain due to re-acceleration play a role. While a study including all these effects is beyond the scope of this work, we note that the energy losses $E dE/dt \simeq -2 \times 10^{-14} \text{GeV}^2/\text{s}$ are balanced by energy gains $E dE/dt = c^2 D_{\text{pp}} \simeq (2Ev_A/3)^2/D(E)$ for Alfvén velocities around 10 km/s. Determining therefore for simplicity $n(z)$ from a station-

ary 1d diffusion equation, the solution is

$$n(z) = n_0 - j_0 \int_0^z \frac{dz'}{D(z')} \quad (4)$$

for a prescribed profile $D(z)$ of the diffusion coefficient. Here, j_0 and n_0 denote the current and the CR electron number density in the Galactic disk, respectively. Choosing an exponential profile for the diffusion coefficient, $D(z) = D_0 \exp(z/z_0)$, the solution becomes

$$n(z) = n_0 + \frac{j_0 z_0}{D_0} [\exp(-z/z_0) - 1]. \quad (5)$$

This solution has two qualitatively different cases: For $j_0 z_0 / D_0 n_0 > 1$, the point $n(z_*) = 0$ defines a free-escape boundary at z_* , while for $j_0 z_0 / D_0 n_0 < 1$ the density $n(z)$ stays non-zero for $z \rightarrow \infty$.

In the subsequent fits, we will fix the z dependence of the CR electron density to the one from of Eq. (5), setting $j_0 z_0 / (D_0 n_0) \simeq 2.0$ together with a minimum value of $n_{\min} = n(z_c) / n_0 = 0.1$. For the magnetic field in the disk, we assume that it is constant with strength B_0 and decreases outwards as $B(z) \propto \exp[-(z - z_0) / z_B]$ for $z > z_{\text{disk}}$ until it reaches the minimal value B_{\min} . Inspired by the relation $B \propto D^{-1/3}$ for Kolmogorov turbulence, we connect the scale heights of the magnetic field to the one of the electron density by $z_B = z_0 / 3$.

V. RESULTS

A. Model parameters and fit procedure

Even our simple toy model contains the 13 parameters shown in Table II that have to be determined in principle from observations. Our aim is however not to find “the best-fit” model, but only to check if a consistent explanation both of the low polarization degree and the synchrotron data is possible. We fix therefore a number of parameters. In particular, we choose for the vertical extension, the coherence lengths, and the vertical scale heights of the electron distribution and the magnetic field the values shown in Table III. Moreover, we fix the normalization of the electron number density, varying only the slope p . For the regular halo field, we neglect the sub-dominant turbulent field and use only a homogeneous field. To add small variations, we divide the halo in 10 patches of size $H_{\text{halo}} / 10$. In each patch, we choose the field direction picking a vector within a cone with opening angle $\vartheta = 15^\circ$ around the initial direction of the homogeneous field.

To find a reasonable fit of the remaining parameters, we use a χ^2 test to fit the latitude profile of the radio intensity at $\nu = 408$ Mhz. We use the $N = 14$ data points presented in Ref. [30] together with the (asymmetric) errors for the radio intensity outside the Galactic disk. We do not add the mean polarization as an additional data point to the χ^2 test: Treating it as a single datum with a

| Parameter | Symbol |
|--|-----------------------|
| Correlation length of corona | $L_{c,\text{corona}}$ |
| Correlation length of disk | $L_{c,\text{disk}}$ |
| Correlation length of halo | $L_{c,\text{halo}}$ |
| Disk field strength | B_0 |
| Electron number density normalization constant | n_0 |
| Electron number density scale height | z_0 |
| Magnetic field strength scale height | z_B |
| Minimum electron number density fraction | n_{\min} |
| Minimum magnetic field strength | B_{\min} |
| Particle distribution index | p |
| Size of corona | H_{corona} |
| Size of disk | H_{disk} |
| Size of halo | H_{halo} |

TABLE II: List of free parameters for the simplified total field model.

| | H/kpc | L_c/kpc | z_B/kpc | z_0/kpc |
|--------|----------------|---------------------|------------------|------------------|
| Disk | 0.2 | 5×10^{-3} | ∞ | 5 |
| Halo | 10 | 10 | 5/3 | 5 |
| Corona | 250 | 50×10^{-3} | 5/3 | 5 |

TABLE III: Parameters of the simplified model.

rather large variance, its weight in the fit would be small. Instead, we calculate the mean polarization towards the Galactic North pole for each fitted case, and consider then only cases below a maximal polarization.

B. Fitting p , z_0 and B_0

For our first χ^2 test, we keep both the minimum electron number density $n_{\min} = 0.1$ and the minimum magnetic field strength $B_{\min} = 0.5 \mu\text{G}$ fixed. This leaves us with three free parameters; p , z_0 and B_0 . We choose seven equally spaced values for $p \in [2.4, 3]$, and five equally spaced values for $z_{t,n} \in [2, 6] \text{ kpc}$ and $B_0 \in [3, 7] \mu\text{G}$. At each latitude we average over 10^3 field realizations. The five best results of the test are summarized in Table IV. The last column of the table also includes the mean degree of polarization for the given parameters, calculated by the line-of-sight integral towards the Galactic north pole.

Values of p close to 2.7 are clearly favored by this test, while the parameters z_0 and B_0 may vary more. The fact that p is well determined is partly a consequence of fixing the normalization of the CR electron density. For the three best fits, Fig. 2 shows the total synchrotron radiation temperature $T = I_\nu c^2 / (2\nu^2 k_B)$ as function of the Galactic latitude l together with the radio data. The best fits for these model give mean polarization degrees around 0.16, which is still quite high. We check therefore how the distribution of these values looks like. In Fig. 3, we show the distribution of Π values for differ-

| p | z_0 [kpc] | B_0 [μG] | n_{\min} | B_{\min} [μG] | χ^2 | $\langle \Pi \rangle$ |
|-----|-------------|-------------------------|------------|------------------------------|----------|-----------------------|
| 2.7 | 2 | 6 | 0.1 | 0.5 | 0.22 | 0.15 |
| 2.7 | 4 | 5 | 0.1 | 0.5 | 0.41 | 0.17 |
| 2.7 | 3 | 5 | 0.1 | 0.5 | 0.47 | 0.15 |
| 2.7 | 6 | 4 | 0.1 | 0.5 | 0.63 | 0.17 |
| 2.7 | 3 | 6 | 0.1 | 0.5 | 0.67 | 0.17 |

TABLE IV: Reduced χ^2 values and mean degree of polarization for the five best set of parameters varying p , z_0 and B_0 ; the parameters n_{\min} and B_{\min} are fixed.

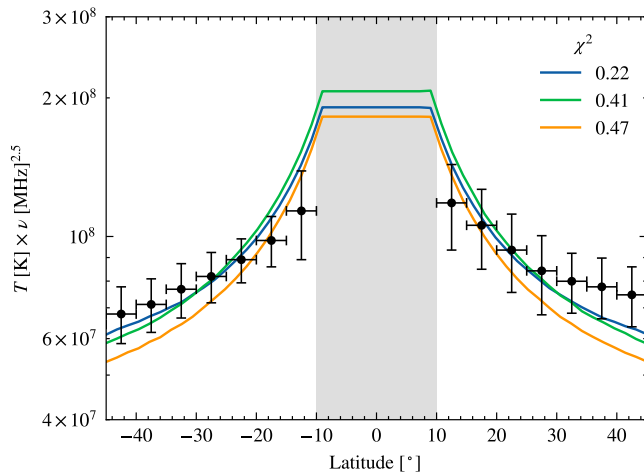


FIG. 2: Latitude profiles of synchrotron emission for the simplified total field model for the three best results from Table IV.

ent realizations of the random field and three value of the slope p of the electron energy distribution. In all the cases shown in Fig. 3, we fix $B_0 = 4\mu\text{G}$ and $z_0 = 5$ kpc. The three distributions have a sharp cutoff at high polarizations and a tail extending to $\Pi = 0$. Decreasing p , the maxima and the cutoffs are shifted as expected to smaller Π values. For $p = 2.8$, the probability to have a random realization with polarization lower than $\Pi \leq 0.05$ is 9%. Similarly, for the three best cases from Table IV there are approximately 20% of cases with polarization less than $\Pi = 0.1$ and 10% of cases less than $\Pi = 0.05$. Thus we conclude that the extremely low polarization observed in the northern C-BASS survey is not typical for our set-up, but happens in a considerable fraction of field realizations.

To understand this behavior better, we show in Fig. 4 the average of the linear polarization fraction Π together with its 1 and 2σ bands as function of the line-of-sight distance s . The left panel illustrates how the polarization degree is reduced as $1/\sqrt{x}$, as the length $s = xL_c$ of the line-of-sight integration increases in the turbulent extended halo field. The same effect is visible for the turbulent disk field in the close-up shown in the right panel. Note also that the 2σ band is very asymmetrical: Depending on the relative orientation of the polarization in

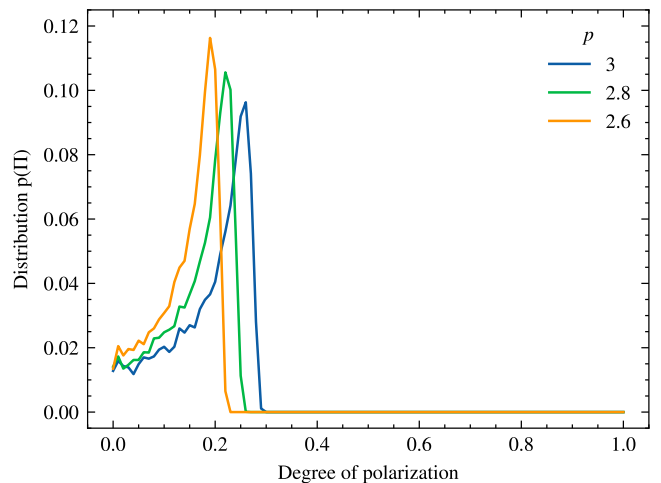


FIG. 3: Distribution of p values for different slopes p of the electron energy distribution, for $B_0 = 4\mu\text{G}$ and $z_n = 5$ kpc.

the disk and the halo, the two contributions can either cancel or sum up. In the first case, the total polarization can become close to zero. Thus very small values of Π require a partial cancellation of the disk and halo contribution to the polarized emission.

C. Fitting p , n_{\min} and B_{\min}

In the second χ^2 test, we want to determine the minimal contribution to the synchrotron intensity required from the extended halo. We therefore consider n_{\min} and B_{\min} together with p as free fit parameters. Decreasing either n_{\min} or B_{\min} increases the polarization degree and decreases the intensity, while on the other hand a smaller value of p corresponds to a higher intensity and lower polarization degree. We will therefore fix the disk field strength $B_0 = 6\mu\text{G}$ and the electron density scale height $z_0 = 2$ kpc, and vary n_{\min} and B_{\min} as well as p .

Choosing six equally spaced values for $p \in [2.65, 2.7]$ and $n_{\min} \in [0.05, 0.1]$, and three equally spaced values for $B_{\min} \in [0.3, 0.5]\mu\text{G}$, gives the results of the χ^2 test presented in Table V. Here, we show the ten latitude fits with a reduced chi-square value less than 0.5; they are sorted by the lowest mean polarization degree. All values obtained for n_{\min} , and B_{\min} are above the minimal values used in the fit range. Thus the results of this fit point towards the need of an extended halo field.

VI. DISCUSSION

We collect here few implications of our results and the model suggested.

- In our fits, we have used Eq. (5) as functional form for the vertical profile of the CR electron density together with $j_0 z_0 / (D_0 n_0) \simeq 2.0$ and the minimal

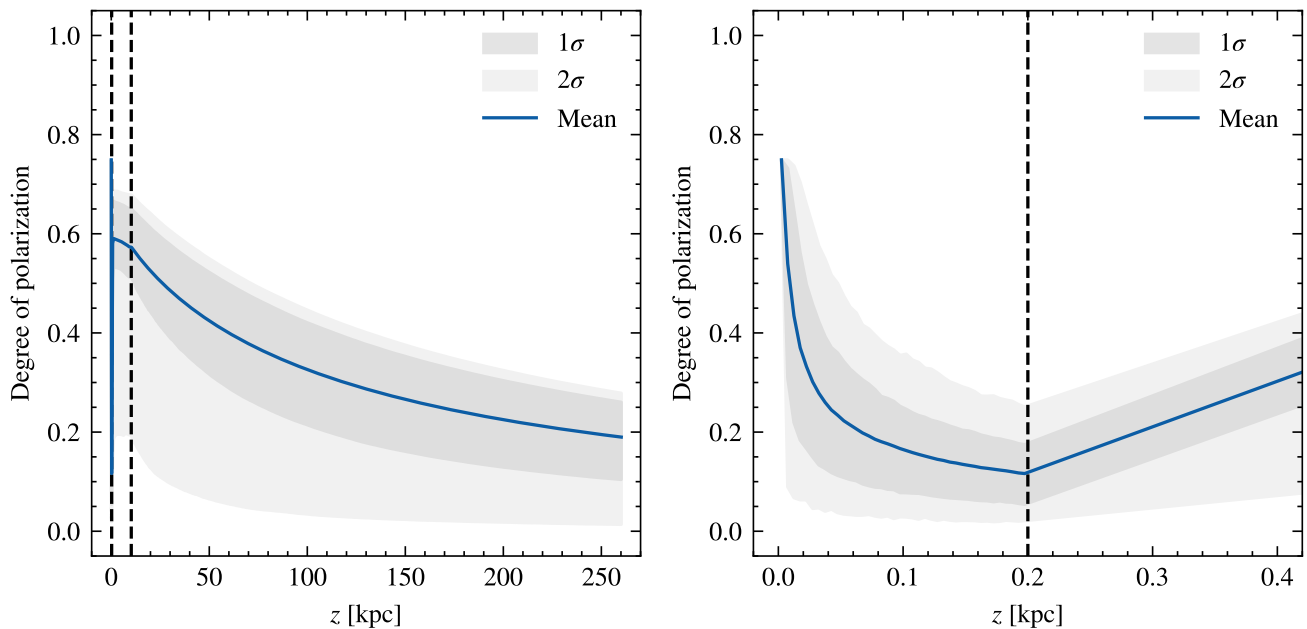


FIG. 4: Linear polarization degree P as function of the L.o.S. distance s .

| p | z_0 [kpc] | B_0 [μG] | n_{\min} | B_{\min} [μG] | χ^2 | $\langle \Pi \rangle$ |
|------|-------------|-------------------------|------------|------------------------------|----------|-----------------------|
| 2.69 | 2 | 6 | 0.1 | 0.5 | 0.37 | 0.15 |
| 2.69 | 2 | 6 | 0.09 | 0.5 | 0.27 | 0.15 |
| 2.7 | 2 | 6 | 0.1 | 0.5 | 0.22 | 0.15 |
| 2.69 | 2 | 6 | 0.1 | 0.4 | 0.19 | 0.16 |
| 2.7 | 2 | 6 | 0.09 | 0.5 | 0.22 | 0.16 |
| 2.67 | 2 | 6 | 0.09 | 0.4 | 0.5 | 0.17 |
| 2.68 | 2 | 6 | 0.08 | 0.5 | 0.43 | 0.17 |
| 2.69 | 2 | 6 | 0.08 | 0.5 | 0.21 | 0.17 |
| 2.68 | 2 | 6 | 0.1 | 0.4 | 0.26 | 0.17 |
| 2.7 | 2 | 6 | 0.1 | 0.4 | 0.35 | 0.17 |

TABLE V: Reduced χ^2 values and mean degree of polarization for varying p , n_{\min} and B_{\min} for the ten best sets of parameters with $\chi^2 < 0.5$ and lowest degree of polarization; the parameters z_0 and B_0 are fixed.

value $n_{\min} = 0.1$. In a more physical way, the latter minimum could be implemented by choosing $j_0 z_0 / (D_0 n_0) \simeq 0.9$. Adjusting then also z_0 to $z_0 = 0.5$ kpc, the profiles for these two choices agree for $|z| \rightarrow 0$. The combination $j_0 / (D_0 n_0)$ of the remaining parameters differs only by a factor of 2.3 between these two cases, indicating that a rather small change in, e.g., the CR luminosity can initiate Galactic outflows which fill up the extended halo with CRs. For a recent study of such a scenario, see Ref. [31].

- Extended halos filled with CR electrons around other Milky Way-like galaxies might lead to detectable radio halos. The intensity of these halos is

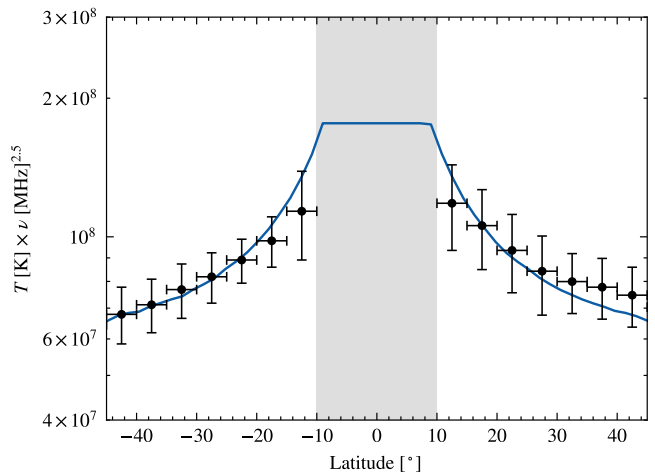


FIG. 5: Total synchrotron radiation temperature T as function of Galactic latitude l .

however low relative to the plane, preventing their detection with current sensitivities [32]: As the intensity scales as $I \propto LnB^2$, one expects a suppression of the halo intensity relative to the peak by $(500/30) \times 0.1 \times (0.5/6)^2 \simeq 0.01$ for a disk diameter of $L = 30$ kpc.

- Fitting observational data, the assumption that only the regular magnetic field contributes to the polarized intensity and the rotation measure, while the turbulent field cancels out completely, does not hold necessarily for realistic conditions. For instance, for $L_{\text{coh}} = L_{\text{max}}/5 = 10$ pc in the disk, and

a disk height of $H = 150$ pc, the turbulent components are suppressed only by $1/\sqrt{15} \sim 0.25$. In reality, the suppression will be even weaker, since the emissivity is not uniform. Thus the regular and turbulent field should be fitted simultaneously to observational data.

- Very small polarization fractions Π require a partial cancellation of the disk and halo contribution. In the case of regular fields, close to perpendicular field lines in and above the disk are however unlikely. In contrast, if the turbulent component dominates in the disk (or at least in the Local Bubble), such a partial cancellation happens naturally in a subset of field realizations.
- An extended magnetic halo can influence the arrival directions and times of ultra-high energy CRs. The rms deflection angle of an iron nucleus in a turbulent field of length d is given by [33]

$$\vartheta = \frac{(2dL_c/9)^{1/2}}{R_L} \quad (6)$$

$$\simeq 23^\circ \left(\frac{10^{20}\text{eV}}{E} \right) \left(\frac{B}{\mu\text{G}} \right) \left(\frac{d}{250\text{ kpc}} \frac{L_c}{50\text{ pc}} \right)^{1/2},$$

while the increased path-length compared to straight-line propagation leads to time-delays

$$\Delta t = \frac{d\vartheta^2}{4} \simeq 1.3\text{Myr} \times \quad (7)$$

$$\left(\frac{10^{20}\text{eV}}{E} \frac{B}{\mu\text{G}} \right)^2 \frac{d}{250\text{ kpc}} \frac{L_c}{50\text{ pc}}.$$

Thus the time delays are even at the highest energies for iron nuclei smaller than the typical activity times of jets in AGN. On the other hand, the halo field induces sizable additional deflections.

- The interactions of CRs confined in the extended magnetic halo of the Milky Way lead to a quasi-isotropic contribution to the photon and neutrino fluxes [34]. We can estimate the ratio of this secondary photon to the CR flux as

$$\frac{I_\gamma(E)}{\langle I_{\text{CR}}(E) \rangle} \simeq H_{\text{cor}} \langle n_{\text{gas}} \rangle \sum_{ij} f_j Z_\gamma^{ij}(p) \sigma_{\text{inel}}^{ij}(E), \quad (8)$$

where f_j is the fraction of proton and helium nuclei in the interstellar gas, $Z_\gamma^{ij}(p)$ is the Z factor for a power-law CR flux with slope p , $\sigma_{\text{inel}}^{ij}(E)$ the inelastic cross section for the production for photons in interactions of CR nuclei of type i on target nuclei j , and $\langle \cdot \rangle$ denotes the average along the line-of-sight. For a rough estimate, we set $\langle n_{\text{gas}} \rangle = 10^{-3}\text{cm}^{-3}$ as average gas density and $\langle I_{\text{CR}}(E, z) \rangle = g I_{\text{CR}}(E, 0)$ with $g \simeq n_{\text{min}} = 0.1$. This results with $H_{\text{cor}} = 250\text{ kpc}$ and $\sum_{ij} f_j Z_\gamma^{ij}(2.6) \sigma_{\text{inel}}^{ij}(E) \simeq$

7.3 mbarn [35] in $I_\gamma(E)/I_{\text{CR}}(E) \simeq 6 \times 10^{-7}$. Thus the secondary photons from CR interactions in the extended halo could give a sizable contribution in the TeV range to the EGRB measured by Fermi-LAT, for a potential signature in the data see Ref. [36]. However, in order to make quantitative statements, more reliable estimates for the gas and CR electron densities are needed. A possible contribution to the diffuse neutrino flux measured by IceCube would be stronger suppressed, first because of the slope $p = 2.6$ and second because the knee in the Galactic CR flux is at an $\simeq 10$ times lower energy than observed locally, as argued in Ref. [37].

- CR Diffusion in the extended Milky Way halo leads to the formation of a magnetic horizon, if $\tau_{\text{esc}} = H_{\text{cor}}^2/(2D) > t_0$ with t_0 as the age of the Universe. In a simplistic picture, the same condition determines the minimal rigidity of extragalactic CRs which can enter the Milky Way. With $\tau_{\text{esc}}(\mathcal{R}) = t_0$, it follows $\mathcal{R} \gtrsim 10\text{ PV}$. Thus a proton component at higher energies than $\simeq 10\text{ PeV}$, where the Galactic protons are already suppressed, might be extragalactic.
- Finally, we note that the different level of turbulence in the disk and halo should lead to differences in the morphology of leptonic gamma-ray sources: While in the disk such gamma-ray halos should be spherical, halos of sources with a rather large vertical distance, $z \simeq 100\text{--}200\text{ pc}$, to the Galactic plane should be elongated along the regular magnetic field lines.

VII. CONCLUSIONS

We have argued that the low linear polarization degree in the northern C-BASS survey together with coherent structures in the polarization over rather large angular scales is incompatible with a uniform ratio of the regular and turbulent magnetic field strengths in the disk and halo of the Milky Way. Since sufficiently fast CR escape requires the dominance of regular fields in the halo, we have suggested the existence of two additional regions dominated by turbulent fields: The disk—which may be only locally dominated by turbulent fields—and an extended halo field. In the extended halo, the field strength and the density of CR electrons should be sufficiently high that the field contributes significantly to the observed synchrotron intensity. In the (local) disk, the ratio of the coherence length and the vertical extension should be such that only a partial cancellation of the disk contribution to the linear polarization degree happens. The extended halo field may lead to sizable additional deflections of UHECRs, while at lower energies interactions of confined Galactic CRs may contribute to the observed diffuse flux of gamma-rays and neutrinos.

Acknowledgments

This work was triggered by a talk of Paddy Leahy at the workshop “Towards a comprehensive model of the Galactic magnetic field” at NORDITA, Stockholm. We would like to thank him and all participants for inspiring discussions. We are grateful to Michael Unger for

useful comments on this draft. MK acknowledges hospitality and financial support by NORDITA for the scientific program “Towards a comprehensive model of the Galactic magnetic field” and by the Bernoulli Center in Lausanne for the scientific program “Generation, evolution, and observations of cosmological magnetic fields”.

-
- [1] R. Beck, A. Brandenburg, D. Moss, A. Shukurov, and D. Sokoloff, *Ann. Rev. Astron. Astrophys.* **34**, 155 (1996).
- [2] F. Boulanger et al., *JCAP* **1808**, 049 (2018), 1805.02496.
- [3] M. S. Pshirkov, P. G. Tinyakov, P. P. Kronberg, and K. J. Newton-McGee, *Astrophys. J.* **738**, 192 (2011), 1103.0814.
- [4] R. Jansson and G. R. Farrar, *Astrophys.J.* **757**, 14 (2012), 1204.3662.
- [5] T. R. Jaffe, K. M. Ferriere, A. J. Banday, A. W. Strong, E. Orlando, J. F. Macias-Perez, L. Fauvet, C. Combet, and E. Falgarone, *Mon. Not. Roy. Astron. Soc.* **431**, 683 (2013), 1302.0143.
- [6] M. Unger and G. R. Farrar (2023), 2311.12120.
- [7] A. Korochkin, D. Semikoz, and P. Tinyakov (2024), 2407.02148.
- [8] R. Beck et al., *aap* **411**, 99 (2003), astro-ph/0307330.
- [9] P. Leahy (2023), talk *Synchrotron constraints on the Galactic magnetic field* at the Workshop “Towards a comprehensive model of the Galactic magnetic field”, NORDITA, Stockholm.
- [10] J. Singal et al., *Publ. Astron. Soc. Pac.* **135**, 036001 (2023), 2211.16547.
- [11] G. Giacinti, M. Kachelrieß, and D. V. Semikoz, *Phys. Rev.* **D90**, 041302 (2014), 1403.3380.
- [12] G. Giacinti, M. Kachelrieß, and D. V. Semikoz, *Phys. Rev.* **D91**, 083009 (2015), 1502.01608.
- [13] G. Giacinti, M. Kachelrieß, and D. V. Semikoz, *JCAP* **1807**, 051 (2018), 1710.08205.
- [14] A. U. Abeysekara et al. (HAWC), *Science* **358**, 911 (2017), 1711.06223.
- [15] G. Jóhannesson et al., *Astrophys. J.* **824**, 16 (2016), 1602.02243.
- [16] T. A. Porter, G. Jóhannesson, and I. V. Moskalenko, *Astrophys. J. Supp.* **262**, 30 (2022), 2112.12745.
- [17] C. Evoli, D. Gaggero, D. Grasso, and L. Maccione, *JCAP* **0810**, 018 (2008), [Erratum: *JCAP*1604,no.04,E01(2016)], 0807.4730.
- [18] P. de la Torre Luque, M. N. Mazziotta, A. Ferrari, F. Loparco, P. Sala, and D. Serini, *JCAP* **07**, 008 (2022), 2202.03559.
- [19] E. Parizot, *Nucl. Phys. Proc. Suppl.* **136**, 169 (2004), astro-ph/0409191.
- [20] A. W. Strong, I. V. Moskalenko, and V. S. Ptuskin, *Ann. Rev. Nucl. Part. Sci.* **57**, 285 (2007), astro-ph/0701517.
- [21] D. de Marco, P. Blasi, and T. Stanev, *JCAP* **06**, 027 (2007), 0705.1972.
- [22] M. Kachelrieß, A. Neronov, and D. V. Semikoz, *Phys. Rev. Lett.* **115**, 181103 (2015), 1504.06472.
- [23] R. Jansson and G. R. Farrar, *Astrophys.J.* **761**, L11 (2012), 1210.7820.
- [24] M. Aguilar et al. (AMS), *Phys. Rev. Lett.* **117**, 231102 (2016).
- [25] R. López-Coto and G. Giacinti, *Mon. Not. Roy. Astron. Soc.* **479**, 4526 (2018), 1712.04373.
- [26] G. Giacinti, M. Kachelrieß, and D. V. Semikoz, *Phys. Rev. Lett.* **108**, 261101 (2012), 1204.1271.
- [27] G. Giacinti, M. Kachelrieß, and D. V. Semikoz, *Phys. Rev.* **D88**, 023010 (2013), 1306.3209.
- [28] P. de la Torre Luque, O. Fornieri, and T. Linden, *PoS ECRS*, 109 (2023).
- [29] D. Bisschoff, M. S. Potgieter, and O. P. M. Aslam, *Astrophys. J.* **878**, 59 (2019), 1902.10438.
- [30] G. Di Bernardo, C. Evoli, D. Gaggero, D. Grasso, and L. Maccione, *JCAP* **03**, 036 (2013), 1210.4546.
- [31] V. N. Zirakashvili, V. S. Ptuskin, and S. I. Rogovaya (2023), 2312.13172.
- [32] M. Krause, J. Irwin, T. Wiegert, A. Miskolczi, A. Damas-Segovia, R. Beck, J.-T. Li, G. Heald, P. Müller, Y. Stein, et al., *Astron. Astrophys.* **611**, A72 (2018), 1712.03780.
- [33] J. Miralda-Escude and E. Waxman, *Astrophys. J.* **462**, L59 (1996), astro-ph/9601012.
- [34] A. M. Taylor, S. Gabici, and F. Aharonian, *Phys. Rev.* **D89**, 103003 (2014), 1403.3206.
- [35] M. Kachelrieß, I. V. Moskalenko, and S. S. Ostapchenko, *Astrophys. J.* **789**, 136 (2014), 1406.0035.
- [36] A. Neronov, M. Kachelrieß, and D. V. Semikoz, *Phys. Rev.* **D98**, 023004 (2018), 1802.09983.
- [37] C. Prevotat, M. Kachelrieß, S. Koldobskiy, A. Neronov, and D. Semikoz (2024), 2407.11911.